Field Reconstruction Modeling Method of a Linear Variable Area Resolver

Authors

Ghasem Salimi Moghaddam[1], Zahra Nasiri-Gheidari[2], Ramin Alipour-Sarabi[3]*

[1]Department of Electrical Engineering, Sharif University of Technology, Tehran, Iran, (ORCID: 0009-0005-0628-9073), ghasem.salimi@alum.sharif.edu

[2]Department of Electrical Engineering, Sharif University of Technology, Tehran, Iran, (ORCID: 0000-0003-0744-1442), znasiri@sharif.edu

[3]Department of Electrical Engineering, K. N. Toosi University of Technology, Tehran, Iran, (ORCID: 0000-0002- 4066-1132), r.alipour@kntu.ac.ir

***Abstract*—Linear resolver is a good candidate for position estimation in severe environments. Performance evaluation of these electromagnetic sensors is a crucial job in the designing process. Due to its 3-D structure, 3-D time-stepping finite element method (FEM) is required for evaluating its performance. However, the simulation time of 3-D FEM is too much, making it unsuitable for design and optimization goals where lots of simulations are needed. Moreover, the quality of the response is affected by the simulation's mesh quality and step time. Therefore, in this paper, the Field Reconstruction Method (FRM) is developed for the evaluation of the proposed sensor. The accuracy and speed of the proposed analytical model are evaluated by 3-D FEM simulations in both AC and DC excitation voltage. Finally, to verify the success of the proposed design and the analytical calculations, the introduced resolver is prototyped and tested. The results show good agreement among the analytical, FEM, and practical assessments**

***Keywords*— Finite Element Method (FEM), Field Reconstruction Method (FRM), Hybrid Resolver, Linear Sinusoidal Area Variable Reluctance Resolver (LSA-VRR), Position Error.**

I. INTRODUCTION

Resolvers, as position sensors, are used in many industrial and robotic motion control systems [1]-[2]. In linear motion applications, both of the rotary and linear resolvers can be used. However, if the rotary resolver is selected, a rotary to linear mechanism, e.g., screw-and-nut system, is needed, as well. Due to the higher performance of direct sensing, linear resolvers are preferred [3].

Linear resolvers similar to the conventional rotary ones are developed in two types: Wound Mover (WM) [3] and Variable Reluctance (VR) [4] types. While in the former excitation winding is used in the moving part, in the latter all windings are installed in the stationary part. Brushes or linear transformers are used in the WM resolvers which make them bulky and costly. Moreover, the impedance of the employed transformer causes phase shift error that needs to be compensated by the Resolver to Digital Converter (RDC). VR resolvers by removing the mentioned elements benefit from a simpler structure. In VR resolvers, the air-gap length [5] or air-gap area [6] varies sinusoidally. VR resolvers with variable air-gap area are more robust to misalignment error compared to VR resolvers with variable air-gap length [7]. Furthermore, they have simpler winding configuration with constant turn non-overlapping coils.

The literature on linear VR resolvers is divided into two main groups. The First category of the literature on VR resolvers is devoted to introducing novel structures [8]-[13]. Although the proposed configurations are innovative, similar to any conventional resolver, they have some shortcomings such as motional voltage error, electromagnetic interference, and high cost. The second group is devoted to modeling of the linear resolvers. The best analytical models should be able to consider the longitudinal end effect, the variations of the air-gap permeance, and the windings' different configurations. The other criterion for the analytical models is their fast but yet reliable response. In [5]-[6] winding function method is used for this purpose. Although it is very fast and can exactly consider the windings' configuration, it ignores the influence of cores' limited dimensions and the air-gap permeance. To fix the weaknesses of the winding function method, Magnetic Equivalent Circuit (MEC) model can be used [14]-[17]. The MEC model usually assumes parallel magnetic flux lines in the air gap length and its accuracy will be questioned in linear VR resolvers due to the use of a limited number of permeances. To increase the accuracy of the MEC model, the authors of [14]-[15] propose an adaptive model with a flexible number of permeances in the air-gap region. In [16]-[17] the co-usage of the MEC model and the conformal mapping is used for accurate modeling of the linear variable air-gap length resolver. The accuracy of the proposed models of [16]-[17] is in an acceptable range, however, they suffer from a relatively high computational burden and they are hardly able to consider 3-D phenomena. Based on the best knowledge of the authors, proposing a fast analytical model that can easily cover all the different important issues of linear VR resolvers has not been investigated up to now. Such shortcomings are

the main motivation of this study. Therefore, the contribution of this paper is to present a fast and at the same time accurate 3-D model to evaluate the performance of linear sinusoidal area variable reluctance resolver.

Accordingly, the approach of this paper to deal with the mentioned challenges is organized as follows: Section II presents the structure of the proposed resolver. Governing the equations of the proposed resolver in AC and DC excitation is discussed in section III. Section IV presents the analytical model of the resolver. Moreover, the simulation FEM results are set forth there. The obtained experimental results of the manufactured resolver are shown in section V. Finally, the paper is concluded in section VI.

II. Structure of the Proposed Resolver

The structure of the proposed resolver and its specifications are shown in Fig. 1(a) and Table I, respectively. The investigated resolver has 10 poles. The primary has 20 teeth; each tooth has a signal coil wrapped in a single layer. The excitation winding is also horizontally placed in the slot that is in the longitudinal direction of the primary. The corresponding winding diagrams are shown in Fig.1 (b).

The mover is designed such that the shared area with the primary slots varies sinusoidally. For this purpose, the equations that describe the position of the two edges of the mover will be as follows:

$$X_u = L \tag{1}$$

$$Y_u = a \cdot \cos(\frac{2\pi P}{L} x) + b \tag{2}$$

$$X_l = 0 \tag{3}$$

$$Y_l = a \cdot \cos(\frac{2\pi P}{L} x) - b \tag{4}$$

Where X_u, Y_u, X_l, Y_l, P and L are the x-axis and y-axis of the upper edge, lower edge, pole pairs, and the length of the primary respectively. While the resolver's moving part moves, the coupling area is changed with the its position x. Fig.2 presents the relative relationship of the moving part and the upper teeth of the primary during the movement. The rectangular area represents the primary's teeth and the circular curves represent the moving part. The graph shows that the coupling area decreases while the secondary moves from position $x = 0$ to $x = \frac{\tau_p}{2} + \frac{b_d}{2}$ where b_d represents the tooth width and τ_p represents the pole pitch. Reluctance of the air-gap can be found as:

$$R = \frac{1}{\mu_0} \cdot \frac{g}{S} \tag{5}$$

Where R is the magnetic reluctance, S is the area of the area of the magnetic flux in the air-gap, and g is the air gap length. The inducted voltage in the signal windings is calculated from equation (6):

$$v = \frac{d\lambda}{dt} = N_s \frac{d\phi}{dt} \quad (6)$$

Where N_s is the turn number of signal windings, and ϕ is the magnetic flux produced by the excitation winding that is calculated from equation (7):

$$\phi = \frac{F}{R} \quad (7)$$

Where F is the magnetomotive force of the excitation winding. From equations (5) to (7), it is concluded that the inducted voltage in the signal windings is determined by two parameters: the coupling area and the air-gap length. So, two different kinds of reluctance resolvers are developed: variable air-gap length and variable coupling area resolvers. The shared area between the moving part and stationary part for i_{th} slot is:

$$S_i = K\cos(\frac{\pi}{\tau_p}x + (i-1)\frac{\pi}{2}) \quad (8)$$

Where K is the maximum shared area. Accordingly, the reluctance of the air gap is:

$$R_i = \frac{1}{\mu_0} \cdot \frac{g}{K\cos(\frac{\pi}{\tau_p}x + (i-1)\frac{\pi}{2})} \quad (9)$$

Therefore, the crossing flux from ith tooth produced with the excitation winding is:

$$\phi_i = \frac{F\mu_0 K}{g}\cos(\frac{\pi}{\tau_p}x + (i-1)\frac{\pi}{2}) \quad (10)$$

Considering the winding arrangements of the signal windings, the linkage flux of the signal windings are:

$$\lambda_s = \sum_{i=1,5,9,13,17} N_s\phi_i - \sum_{i=3,7,11,15,19} N_s\phi_i \quad (11)$$

$$\lambda_c = \sum_{i=2,6,10,14,18} N_s\phi_i - \sum_{i=4,8,12,16,20} N_s\phi_i \quad (12)$$

SIN and COS windings are the same, but they are 90 degrees electrical displacement relative to each other. Replacing the turn function of signal windings in equations (11) and (12), and using equation (6), the induced voltages are:

$$v_s = \frac{d\lambda_s}{dt} = V_m \sin(\frac{\pi}{\tau_p}x) \quad (13)$$

$$v_c = \frac{d\lambda_c}{dt} = V_m \cos(\frac{\pi}{\tau_p}x) \quad (14)$$

III. GOVERNING EQUATIONS

By applying an AC voltage V_e to the excitation winding, V_s and V_c will be inducted in the signal windings, such that:

$$v_e = \mathrm{R_e}\, i_e + \frac{d\psi_e}{dt} \quad (15)$$

$$v_s = \mathrm{R_s}\, i_s + \frac{d\psi_s}{dt} \quad (16)$$

$$v_c = \mathrm{R_c}\, i_c + \frac{d\psi_c}{dt} \quad (17)$$

Where R_e, R_s, and R_c are excitation, sinuous, and co-sinuous windings resistance, respectively. The signal windings are connected to RDC whose input impedance is high. Accordingly, the signal winding currents, that are i_s and i_c, are negligible. Flux linkage with the excitation, sinuous, and co-sinuous windings are, respectively:

$$\psi_e = L_{ex} i_e \quad (18)$$

$$\psi_s = L_{se} i_e \quad (19)$$

$$\psi_c = L_{ce} i_e \quad (20)$$

where, L_{ex} is the excitation winding self-inductance and L_{se} and L_{ce} are the mutual-inductance between excitation and signal windings. Resolvers are designed such that the excitation winding's self-inductance is not affected by the position of the moving part [3]. The mutual-inductance of the excitation and signal windings in the ideal form are sinusoidal function of the moving part, such that:

$$L_{se} = M_m \sin(\frac{\pi}{\tau_p} x) \quad (21)$$

$$L_{ce} = M_m \cos(\frac{\pi}{\tau_p} x) \quad (22)$$

where M_m is the maximum value of the mutual-inductance, τ_p is the pole pitch, and x is the moving part position.

1) AC Excitation

When the excitation winding is fed with a sinusoidal voltage, the winding current, i_e, will be AC, too. Therefore, the signal windings' flux linkage in this condition are:

$$\psi_s = M_m \sin(\frac{\pi}{\tau_p} x) \times (I_e \sin(\omega_e t + \theta_e)) \quad (23)$$

$$\psi_s = M_m \cos(\frac{\pi}{\tau_p} x) \times (I_e \sin(\omega_e t + \theta_e)) \quad (24)$$

Where I_e is the maximum current of excitation winding current, ω_e is the angular frequency of current, and θ_e is the phase shift of the excitation winding current resulting from its impedance. The inducted voltages in the signal windings are:

$$v_s = \frac{d\psi_s}{dt} = M_m I_e \left(\frac{\pi}{\tau_p}\frac{dx}{dt}\cos\left(\frac{\pi}{\tau_p}x\right)\sin(\omega_e t) + \omega_e \sin\left(\frac{\pi}{\tau_p}x\right)\cos(\omega_e t)\right) \quad (25)$$

$$v_c = \frac{d\psi_c}{dt} = M_m I_e \left(-\frac{\pi}{\tau_p}\frac{dx}{dt}\sin\left(\frac{\pi}{\tau_p}x\right)\sin(\omega_e t) + \omega_e \cos\left(\frac{\pi}{\tau_p}x\right)\cos(\omega_e t)\right) \quad (26)$$

Replacing the mover velocity, $V_m = \frac{dx}{dt}$, in equations (25) and (26), and assuming $\frac{V_m}{\omega_m} \ll 1$, the voltage equations are simplified as:

$$v_s \cong M_m \omega_e I_e \sin\left(\frac{\pi}{\tau_p}x\right)\cos(\omega_e t) \quad (27)$$

$$v_c \cong M_m \omega_e I_e \cos\left(\frac{\pi}{\tau_p}x\right)\cos(\omega_e t) \quad (28)$$

Accordingly, the inducted voltages are amplitude-modulated (AM) signals. Finally, the instantaneous position is calculated:

$$x \cong \frac{\tau_p}{\pi}\tan^{-1}\left(\frac{v_s}{v_c}\right) \quad (29)$$

2) DC Excitation

When the excitation winding is fed with a DC voltage, the winding current, i_e, will be DC, too. Therefore, the signal windings' flux linkage in this condition are:

$$\psi_s = M_m \sin\left(\frac{\pi}{\tau_p}x\right)\cdot I_e \quad (30)$$

$$\psi_c = M_m \cos\left(\frac{\pi}{\tau_p}x\right)\cdot I_e \quad (31)$$

By derivation of the flux linkage equation, the inducted voltages are calculated:

$$v_s = \frac{d\psi_s}{dt} = M_m I_e \frac{\pi}{\tau_p}\frac{dx}{dt}\cos\left(\frac{\pi}{\tau_p}x\right) \quad (32)$$

$$v_c = \frac{d\psi_c}{dt} = -M_m I_e \frac{\pi}{\tau_p}\frac{dx}{dt}\sin\left(\frac{\pi}{\tau_p}x\right) \quad (33)$$

Accordingly, the induced voltages are a sinusoidal function of the mover position. Therefore, the instantaneous position can be calculated as:

$$x = \frac{\tau_p}{\pi} \cot^{-1}(-\frac{v_s}{v_c}) \tag{34}$$

$$x = \frac{\tau_p}{\pi} (\frac{\pi}{2} - \tan^{-1}(\frac{v_c}{v_s})) \tag{35}$$

IV. Analytical Model of LSA-VRR

The design and optimization of the sensor to achieve the desired output requires a repetitive process. Although finite elements analysis (FEA) is a precise method for checking the performance of electric machines, this method is a very time-consuming process, especially in structures that require three-dimensional (3D) analysis, Therefore, it cannot be used in the design stage. In this section, an analytical model based on the field reconstruction method is presented for the LSA-VR resolver.

The field reconstruction method has been used for the first time to minimize the torque ripples of the permanent magnet synchronous machine. For this purpose, several static finite element analyses have been conducted to calculate the basic functions [18]. This method is used for switch reluctance [19], axial flux [20]-[22], and, tubular machines [23].

The basis of the field reconstruction method is based on the symmetries in the structure. In this method, it is assumed that the equations are linear. In this essence, supper position principal is used that takes advantage of fast evaluation response. In resolvers, the rate of magnetic flux is about some tense of milli weber that makes the assumption valid for this application. In this method, the required specifications are calculated in limited states using finite element simulation, and using these results, the performance of the sensor can be described in other situations as well. In the conventional FRM, the tangential and vertical components of air gap flux density are used as basic functions to predict the machine's performance. But considering that only the excitation current and the inducted voltages in the signal windings are needed to predict the performance in the resolver, instead of the magnetic field components of the air gap, the self and mutual inductances of the windings are used as basic functions. Since the current of the signal windings in the resolver is almost zero, they have no effect on the magnetic field, and the only source of field generation is the excitation winding current. Fig. 3 shows magnetic flux distribution in the air-gap before and after the displacement of the secondary for one slot pitch. Ignoring the field caused by the signal windings, the excitation winding magnetic field is repeated as the secondary moves as one slot pitch. Accordingly, by moving the secondary for one slot pitch, it is possible to calculate the inductances of the excitation coils for a complete mechanical

cycle. As the basic functions are derived from FEA, it is possible to improve mesh quality in order to obtain more accurate results. In fact, the partial FEA in the field reconstruction method makes it possible to increase the accuracy of the analytical results by improving the meshing quality, which is time-consuming and costly in complete FEM.

The map of mesh for the investigated resolver is shown in Fig. 4.

The FEM simulations have been done through Ansys/Maxwell software. The total number of mesh elements in the primary and the secondary are 166771 and 138283 respectively. The largest mesh element length is 0.25 mm. Also, the step-time of simulations is 12.5 microseconds.

In the studied resolver, when the secondary part moves a complete mechanical transition, the flux of the stator teeth will have a phase difference equal to one slot pitch. Therefore, by calculating the mutual inductance of the excitation winding and the coil of the signal winding around each tooth of the primary, and summing them, the total mutual inductance is derived. By applying $\boldsymbol{I}_{test}$ to the excitation winding in FEA, the excitation winding self-inductance $L_{ex}^{FEA}(x)$ and the mutual inductance with a single turn of the i^{th} coil of the signal windings $M_i^{FEA}(x)$ when the mover is in x position is obtained, such that:

$$L_{ex}^{FEA}(x); 0 \le x < \frac{l}{Z_s} \tag{36}$$

$$M_i^{FEA}(x); 0 \le x < \frac{l}{Z_s}; i = 1, 2, ..., Z_s \tag{37}$$

where l and Z_s are the length and the number of slots of the primary. The self-inductance of the excitation winding for the slot j is calculated through:

$$L_{ex}(x) = L_{ex}^{FEA}(x - \frac{l}{Z_s}(j-1)); \frac{l}{Z_s}(j-1) \le x < \frac{l}{Z_s} j \tag{38}$$

The mutual-inductance of the excitation winding and 1st coil of the signal winding is calculated as:

$$M_1(x)=\begin{cases} M_1^{FEM}(x); & 0\le x<\dfrac{l}{Z_s} \\ M_2^{FEM}(x-\dfrac{l}{Z_s}); & \dfrac{l}{Z_s}\le x<\dfrac{2l}{Z_s} \\ M_3^{FEM}(x-\dfrac{2l}{Z_s}); & \dfrac{2l}{Z_s}\le x<\dfrac{3l}{Z_s} \\ \vdots & \vdots \\ M_{Z_s}^{FEM}(x-(Z_s-1)\dfrac{l}{Z_s}); & l-\dfrac{l}{Z_s}\le x<l \end{cases} \tag{39}$$

Accordingly, the mutual-inductance with the i^{th} coil of the signal winding is obtained:

$$M_i(x)=M_1(x-(i-1)\frac{l}{Z_s});0\le x<\frac{l}{Z_s} \tag{40}$$

Finally, the total mutual-inductance (for all the coils) of the signal winding is:

$$M(x)=\sum_1^{Z_s} N_i M_i(x);0\le x<\frac{l}{Z_s} \tag{41}$$

where, N_i is the turn number of the i^{th} coil of the signal winding. To find the inducted voltage in the signal windings, the excitation current must be calculated. Form (5) and (8) one can find that:

$$v_{ex}(t)=\mathrm{R_e}\, i_e(t)+\frac{d}{dt}(L_{ex}(x(t))i_e(t)) \tag{42}$$

By the aid of the second-order Runge-Kutta method, the excitation current is calculated as:

$$i_e^{k+1}=\frac{v_e^k+v_e^{k+1}}{2}\frac{\Delta t}{L_{ex}^{k+1}+R\dfrac{\Delta t}{2}}+i_e^{k+1}\frac{L_{ex}^k-R\dfrac{\Delta t}{2}}{L_{ex}^{k+1}+R\dfrac{\Delta t}{2}} \tag{43}$$

Form equations (16), (17), (19), and (20) the induced voltage can be written as:

$$v_{signal}(t)\cong\frac{d}{dt}(M(x(t))i_e(t)) \tag{44}$$

By the aid of the Backward Euler method, the inducted voltages in the signal windings are calculated as:

$$v_{signal}^{k+1}=\frac{M_{signal}^{k+1}i_e^{k+1}-M_{signal}^{k}i_e^{k}}{\Delta t} \tag{45}$$

Note that FRM does not require joint simulation with FEM. In fact, in the first stage, FEM simulation with a limited motion is carried out. The results of limited 3-D FEM simulations are saved and in the post processing stage, (26)-(31), the complete results are extracted. This two-stage process is called FRM. Figs. 5, and 6 show FRM and FEM results with AC excitation and when the mover speed is 1 m/s and 5 m/s, respectively. Similar results for the DC excitation are shown in Figs. 7 and 8. Investigations show that even though there is not much difference between FRM results and FEM results, considerable time saving is done. Both of the FRM and FEM analyses are done on personal computer with 32 GB memory, Core i7 6700HQ CPU, and 64-bit operating system. Table II presents a brief comparison of the two simulations time. Results show a considerable reduction in time and, consequently, cost when the field reconstruction method is used. As an example, in AC excitation and 1m/s mover speed, FRM is about 173.5 times faster than FEM. In similar condition but DC excitation, FRM is about 34.5 times faster than FEM. The origin of this faster simulation is that in FRM larger time step can be selected. While in FEM the sampling frequency is about 16 to 20 times the excitation winding frequency, in FRM the sampling frequency is selected about that of the excitation winding. Moreover, the secondary needs to be moved for only one slot pitch, that is 5 mm for this resolver. Accordingly, the computational burden of FRM is too lower than that of FEM. To do such modeling in FRM, 25 Magnetostatics simulations are done. It is worth noting that the total data in FRM is about 1.26 GBs which is 1/20 that of a complete 3-D FEM one.

V. PRACTICAL EVALUATION

To verify the accuracy of the analytical model, an LSA-VR resolver is manufactured and tested. Fig. 9 shows the primary and the secondary of the manufactured resolver.

The test system is shown in Fig. 10, as well. The different parts of this test system are as below:

1. Function Generator to feed the excitation winding,
2. Oscilloscope to capture the inducted voltages in the signal windings,
3. DC Power Supply to feed the DC Motor,
4. DC Motor to move the secondary,
5. Linear Encoder
6. Primary
7. Secondary

A function generator is used to feed the excitation winding. To move the secondary a brushed permanent magnet DC motor is used. So, a DC power supply is needed to run the motor. Besides DC power supply is used in the DC mode excitation. Induced voltages in the signal windings are captured with an oscilloscope

and analyzed in computer. The length of primary is 105mm and the height of them is 5 mm and 10 mm, respectively. The machine has 20 slots for signal windings with 1.75 mm and 2.25 mm width and depth, respectively. The excitation winging is grooved in the middle of the secondary that has 3.50 mm depth and 3.64 mm width. Excitation winding is fed with 5 volts and 5kHz in AC and 10 volts in DC excitation modes. The winding diagram of this 10-pole resolver is shown in Fig. 1(b).

Test is done in 1m/s and 2 m/s for AC excitation and 4 m/s, and 5 m/s with DC excitation. Figs. 11 and 12 show the inducted voltages in AC and DC excitation, respectively. Average of absolute position error (AAPE) and maximum position error (MPE) are extracted and compared at different speeds. Fig. 13 presents a comparison of estimated position error in AC and DC excitations, respectively. There is an acceptable agreement between the practical results and the analytical ones. As an example, in AC excitation when the mover speed is 1m/s, the deviation of the calculated AAPE by FRM and FEM from the measured value, is 8.5% and 8.9%, respectively. Similarly, in DC excitation when the mover speed is 5m/s, the deviation of the calculated AAPE by FRM and FEM from the measured value, is 8.24% and 7.92%, respectively. Close agreement between the measured results and those of simulations approves the success of the proposed design and the developed analytical model.

VI. Conclusion

In linear motion systems, linear position measurement is preferred. Linear resolvers, due to their electromagnetic structure are more accurate in harsh environments. Among different types of resolvers, variable reluctance ones have a simple structure. Accordingly, in this paper liner sinusoidal area variable reluctance resolver for a wide velocity range was introduced. Performance evaluation and improvement is a necessary job in the design process that is usually done by FEM software. However, multiple simulations in the optimization process makes it almost impossible to use numerical methods. In this essence, a hybrid method that uses analytical and numerical methods at the same time, namely field reconstruction method, was suggested and used in this paper. Comparing FEM and FRM results in AC and DC excitation showed the efficiency of the proposed method in fast and accurate modeling. To verify the simulation modeling an LSA-VR resolver was manufactured and tested. The practical results approved the simulations and modeling. This model will be used to design and optimize the proposed resolver for a wide velocity range.

Acknowledgment

This work is based upon research funded by Iran National Science Foundation (INSF) under project No. 4020661 and Sharif University of Technology.

REFERENCES

[1] Ran, X., Shang, M., et al., "Improved configuration proposal for axial reluctance resolver using 3-d magnetic equivalent circuit model and winding function approach," *IEEE Transactions on Transportation Electrification*, **9**, pp. 311-321, (2023). DOI: 10.1109/TTE.2022.3199538.

[2] Gundogdu, T., "Design of limited-angle wound rotor resolvers for high accuracy and easy manufacturability," *IEEE Transactions on Transportation Electrification*, **9**, pp. 2544-2556, (2023). DOI: 10.1109/TTE.2022.3208358.

[3] Faryadras, R. and Tootoonchian, F., "Design and experimental investigation of a two-dof planar resolver," *IEEE Transactions on Instrumentation and Measurement*, **71**, pp. 1-8, (2022). DOI: 10.1109/TIM.2021.3139656.

[4] KhajueeZadeh, M. S., and Tootoonchian, F., "Developing a very fast and accurate model of linear sinusoidal area resolver considering end-effects and faulty conditions," *IEEE Sensors Journal*, **23**, pp. 2147-2154, (2023). DOI: 10.1109/JSEN.2023.3300838.

[5] Daniar, A., Nasiri-Gheidari, Z., and F. Tootoonchian, "Performance analysis of linear variable reluctance resolvers based on an improved winding function approach," *IEEE Transactions on Energy Conversion*, **33**, pp. 1422-1430, (2018). DOI: 10.1109/TEC.2018.2813335.

[6] Bahari, M., Alipour-Sarabi, R., Nasiri-Gheidari, Z., and F. Tootoonchian, "Proposal of winding function model for geometrical optimization of linear sinusoidal area resolvers," *IEEE Sensors Journal*, **19**, pp. 5506-5513, (2015). DOI: 10.1109/JSEN.2019.2908926.

[7] Shang, J., Wang, H., Chen, M., et al. "The effects of stator and rotor eccentricities on measurement accuracy of axial flux variable-reluctance resolver with sinusoidal rotor," in *2014 17th International Conference on Electrical Machines and Systems (ICEMS)*, Hangzhou, China, pp. 2004-2007, (2014). DOI: 10.1109/ICEMS.2014.7013814.

[8] Ramezannezhad, A., Naderi, P., and Vandevelde, L., "A novel method for accuracy improvement of variable reluctance linear resolvers," *IEEE Sensors Journal*, **22**, pp. 18409-18417, (2022). DOI: 10.1109/JSEN.2022.3199807.

[9] Ramezannezhad, A., Naderi, P., and Vandevelde, L., "A linear position sensor proposal by development of a variable reluctance linear resolver," *2022 30th International Conference on Electrical Engineering (ICEE)*, Tehran, Iran, pp. 570-576, (2022). DOI: 10.1109/ICEE55646.2022.9827303.

[10] Faryadras, R. and Tootoonchian, F., "Design and experimental investigation of a two-dof planar resolver," *IEEE Transactions on Instrumentation and Measurement*, **71**, pp. 1-8, (2022). DOI: 10.1109/TIM.2021.3139656.

[11] Sun, L., Taylor, J., Callegaro, A.D., and Emadi, A., "Stator-pm-based variable reluctance resolver with advantage of motional back-emf," *IEEE Transactions on Industrial Electronics*, **67**, pp. 9790-9801, (2020). DOI: 10.1109/TIE.2019.2955410.

[12] Ghandehari, R., Naderi, P., and Vandevelde, L., "Performance analysis of a new type pm-resolver in healthy and eccentric cases by an improved parametric mec method," *IEEE Transactions on Instrumentation and Measurement*, **70**, pp. 1-10, (2021). DOI: 10.1109/TIM.2021.3080388.

[13] Sun, L., Luo, Z., Wang, K., et al. "A Stator-pm resolver with field modulation principle," *IEEE Transactions on Energy Conversion*, **36**, pp. 159-172, (2021). DOI: 10.1109/TEC.2020.3001655.

[14] Naderi, P., Ramezannezhad, A., and Vandevelde, L., "Performance analysis of variable reluctance linear resolver by parametric magnetic equivalent circuit in healthy and faulty cases," *IEEE Sensors Journal*, **21**, pp. 19912-19921, (2021). DOI: 10.1109/JSEN.2021.3094798.

[15] Naderi, P., Ramezannezhad, A., and Vandevelde, L., "A novel linear resolver proposal and its performance analysis under healthy and asymmetry air-gap fault," *IEEE Transactions on Instrumentation and Measurement*, **71**, pp. 1-9, (2022). DOI: 10.1109/TIM.2022.3155747.

[16] Keyvannia, A., Zare, F., and Tootoonchian, F., "Analytical modeling of variable-reluctance tubular resolver based on magnetic equivalent circuit and conformal mapping," *IEEE Transactions on Instrumentation and Measurement*, **70**, pp. 1-8, (2021). DOI: 10.1109/TIM.2021.3119141.

[17] Seyed-Bouzari, S.A., Saneie, H., and Nasiri-Gheidari, Z., "Analysis and compensation of the longitudinal end-effect in variable reluctance linear resolvers using magnetic equivalent circuit model," *IEEE Transactions on Transportation Electrification*, **9**, pp. 3970-3977, (2023). DOI: 10.1109/TTE.2023.3239500.

[18] Weidong, Z., Fahimi, B., and Pekarek, S., "A field reconstruction method for optimal excitation of permanent magnet synchronous machines" *IEEE Transactions on Energy Conversion*, **21**, pp.305-313, (2006). DOI: 10.1109/TEC.2005.859979.

[19] Lin, C., Wang, W., McDonough, M., et al. "An extended field reconstruction method for modeling of switch reluctance machines," *IEEE Transactions on Magnetics*, **48**, pp.1051-1054, (2012). DOI: 10.1109/TMAG.2011.2172917.

[20] Ajily, E., Abbaszadeh, K., and Ardebili, M., "Three-dimensional field reconstruction method for modeling axial flux permanent magnet machines," *IEEE Transactions on Energy Conversion*, **30**, pp.199-207, (2015). DOI: 10.1109/TEC.2014.2353299.

[21] Ajily, E., Ardebili, M., and Abbaszadeh, K., "Magnet defect and rotor eccentricity modeling in axial-flux permanent-magnet machines via 3-d field reconstruction method," *IEEE Transactions on Energy Conversion*, **31**, pp.486-495, (2016). DOI: 10.1109/TEC.2015.2506819.

[22] Park, H. J., Jung, H.-K., Jung, S.-Y., et al. "Field reconstruction method for axial flux permanent magnet motor with overhang structure," *IEEE Transactions on Magnetics*, **53**, pp.1-4, (2017). DOI: 10.1109/TMAG.2017.2653839.

[23] Kim, K. H., and Woo, D.-K., "Field reconstruction method for linear tubular permanent magnet motor," *IEEE Access*, **8**, pp.169516-169524, (2020). DOI: 10.1109/ACCESS.2020.3023907.

LIST OF FIGURES

LIST OF TABLES

FIGURES AND TABLES

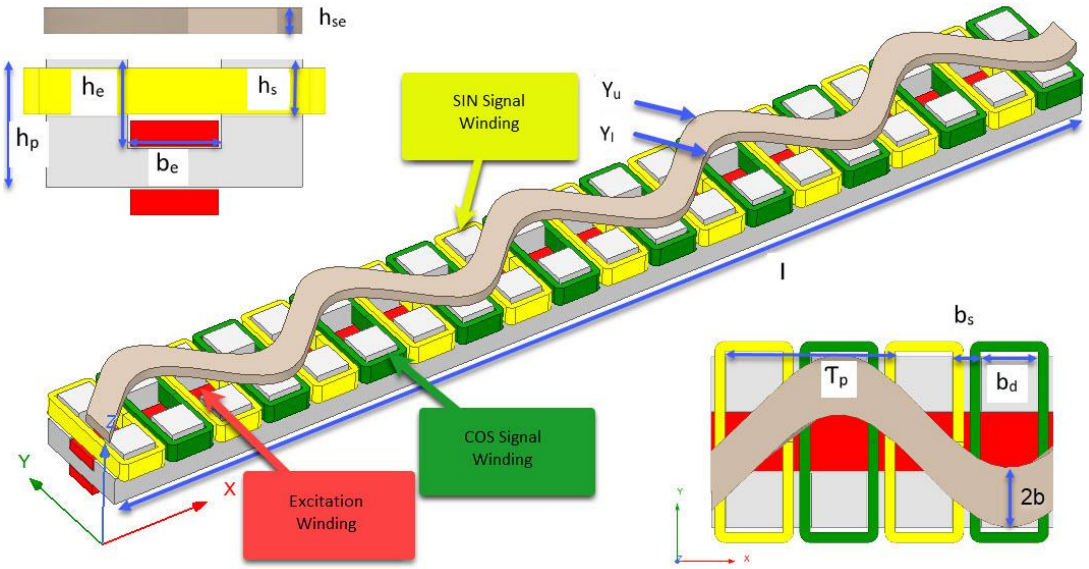

(a)

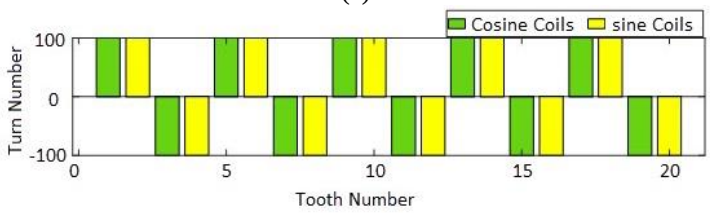

(b)

Fig. 1. (a): Structure of LSA-VRR, (b): Turn number of signal coils based on the primary tooth number

TABLE I: PARAMETERS OF PROPOSED RESOLVER

Parameter	Unit	Value
Primary/ Secondary Height (h_p/h_{se})	mm	5 / 10
Primary Length (l)	mm	105
No. Pole Pairs (p)	--	5
Pole Pitch (τ_p)	mm	10
Signal Winding Slot/Tooth Width (b_s/b_d)	mm	1.75 /3.25
Signal Winding Slot Depth (h_s)	mm	2.25
No. of Slots	---	20
Excitation Winding Slot Depth/ Width (h_e/b_e)	mm	3.50/3.64
Signal Winding No. of Turn Per Phase	---	100
Excitation Number of Turn (N_e)	---	100
DC/AC Excitation Voltage Amplitude	V	5/10
AC Excitation Frequency	Hz	5000

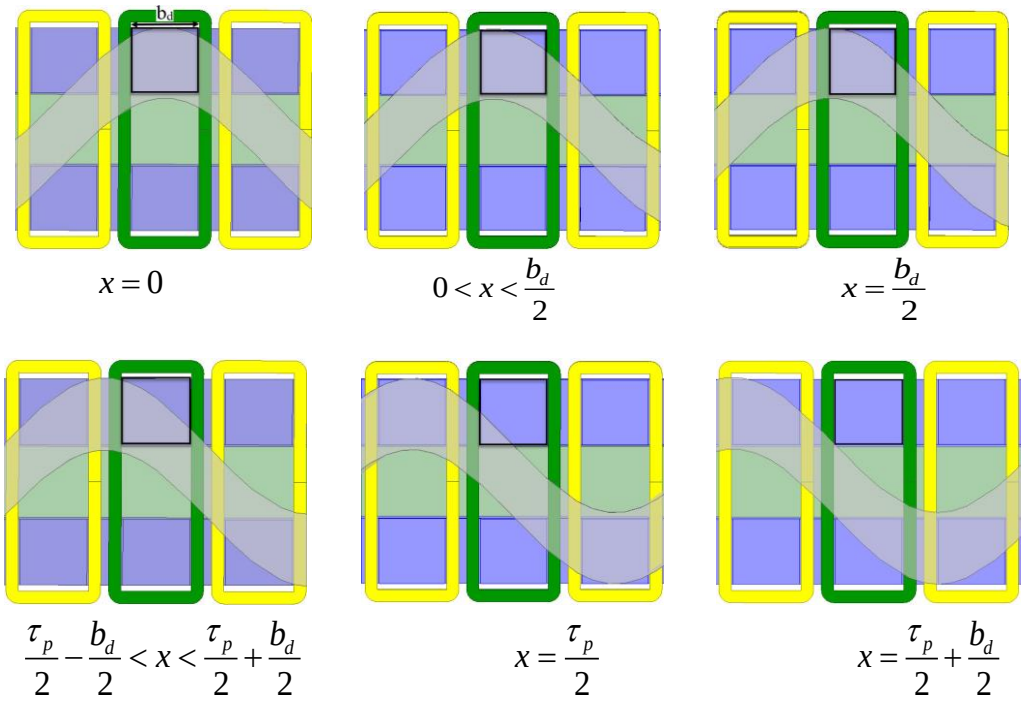

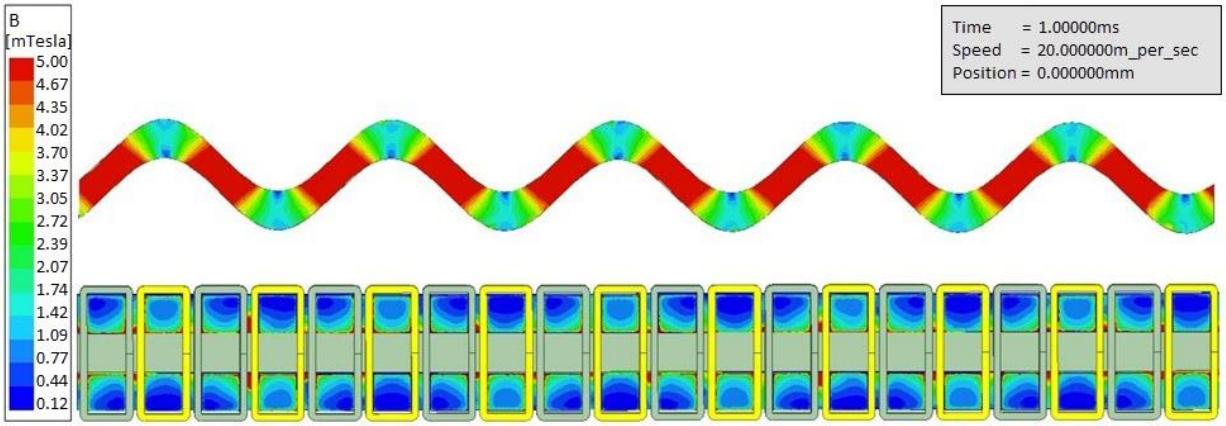

(a)

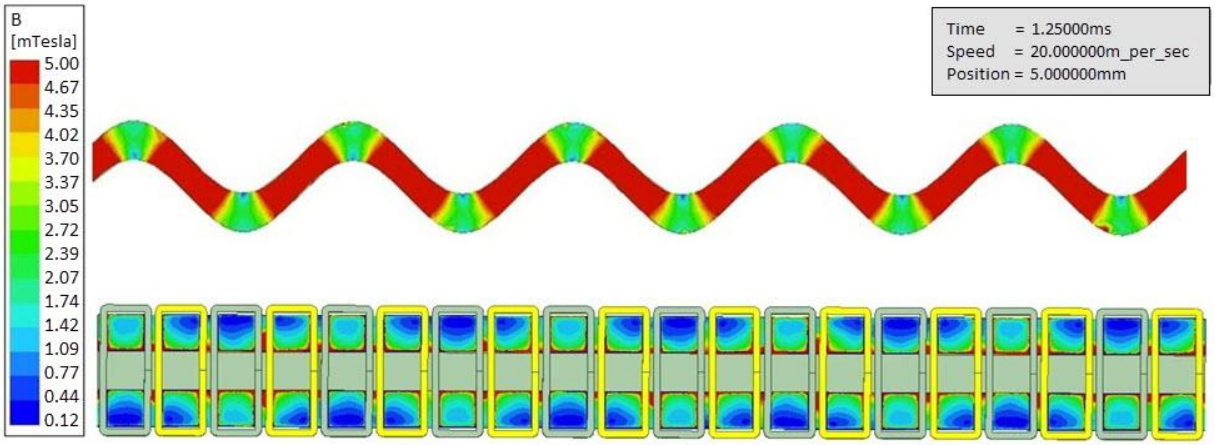

(b)

Fig. 3. Magnetic flux distribution in the air-gap, (a): Initial position, (b): after one slot pitch displacement

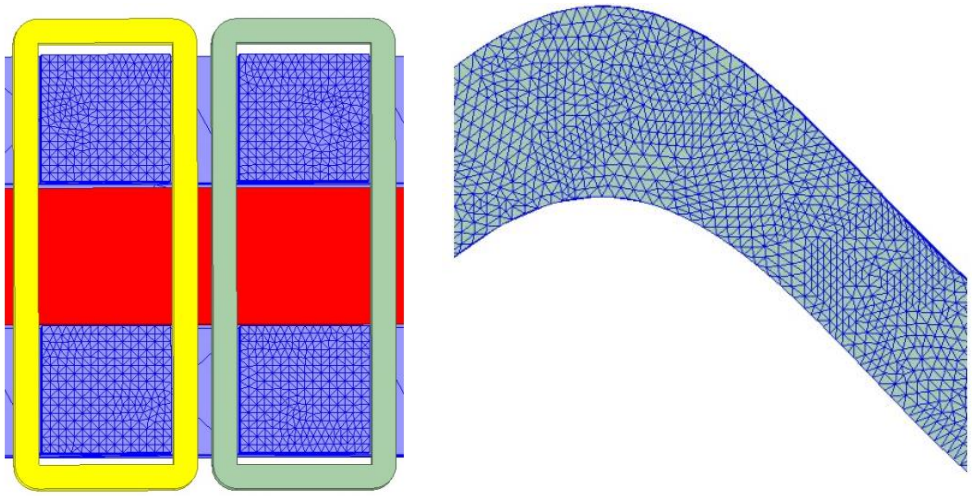

(a) (b)

Fig. 4. Mesh mapping for Finite Element Analysis, (a): Primary, (b): Secondary

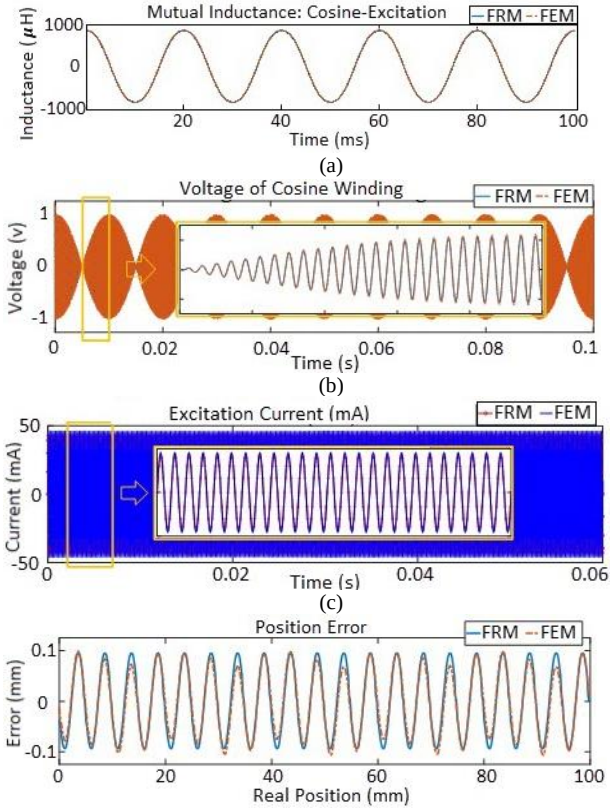

Fig. 5 FRM and FEM results comparison in AC excitation and speed of 1 m/s, (a): Mutual inductance, (b): Inducted voltage, (c): Excitation current, (d): Estimated position error

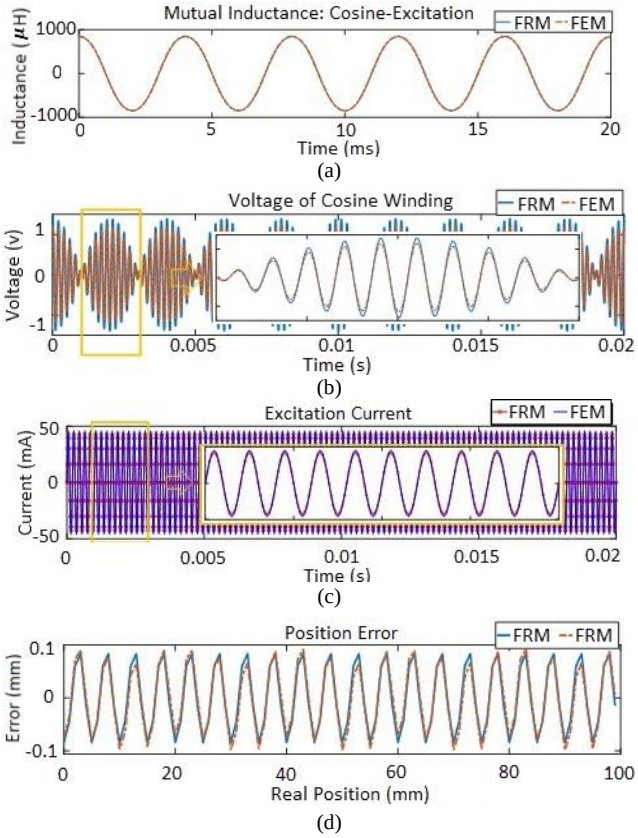

Fig. 6. FRM and FEM results comparison in AC excitation and speed of 5 m/s, (a): Mutual inductance, (b): Inducted voltage, (c): Excitation current, (d): Estimated position error

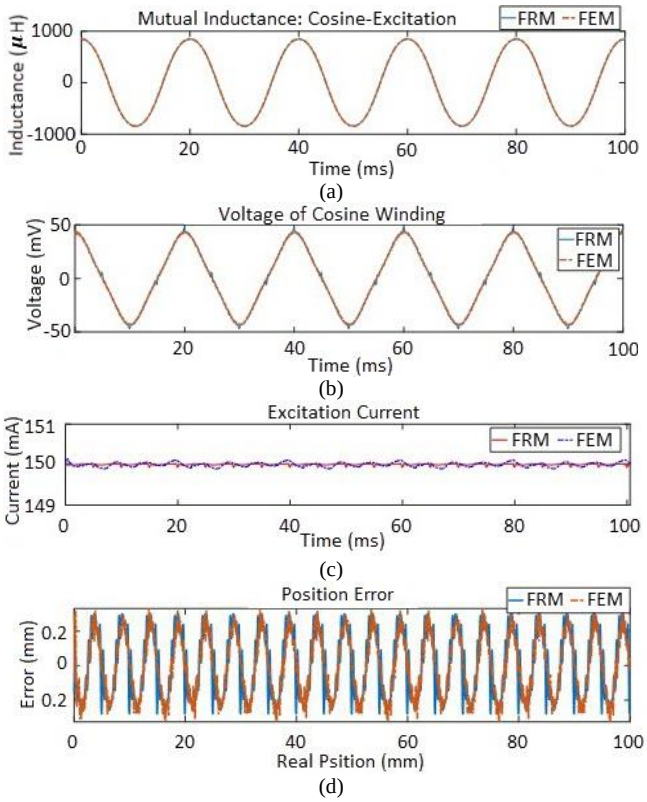

Fig. 7. FRM and FEM results comparison in DC excitation and speed of 1 m/s, (a): Mutual inductance, (b): Inducted voltage, (c): Excitation current, (d): Estimated position error

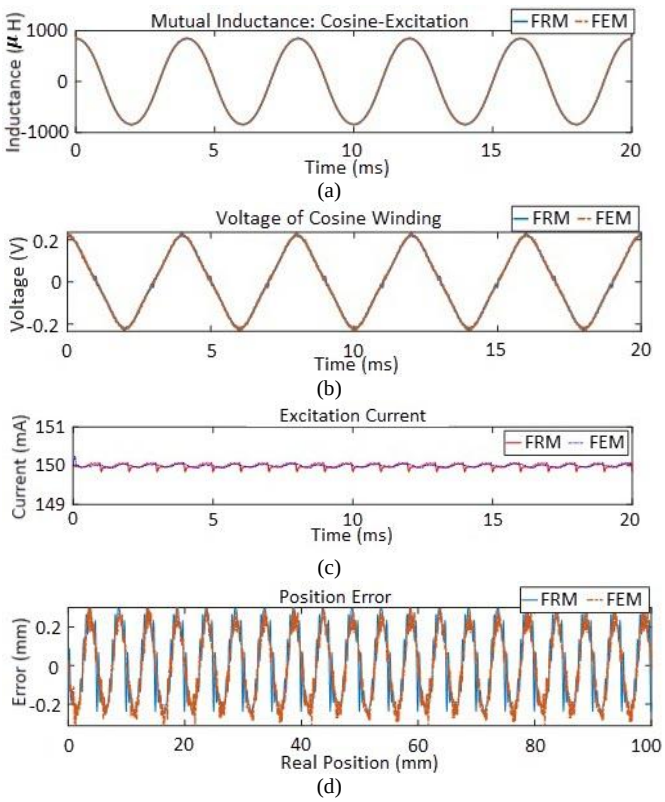

Fig. 8. FRM and FEM results comparison in DC excitation and speed of 5 m/s, (a): Mutual inductance, (b): Inducted voltage, (c): Excitation current, (d): Estimated position error

TABLE II: FRM AND FEM SIMULATION DURATION COMPARISON

	Mover Speed	Method	Duration
AC Excitation	1 (m/s)	FRM	1 h. and 40 min.
		FEM	289 h. and 50 min.
	5 (m/s)	FRM	1 h. and 40 min.
		FEM	58h. 10 min.
DC Excitation	1 (m/s)	FRM	1 h. and 40 min.
		FEM	288 h. 20 min.
	5 (m/s)	FRM	1 h. and 40 min.
		FEM	57 h. 40 min.

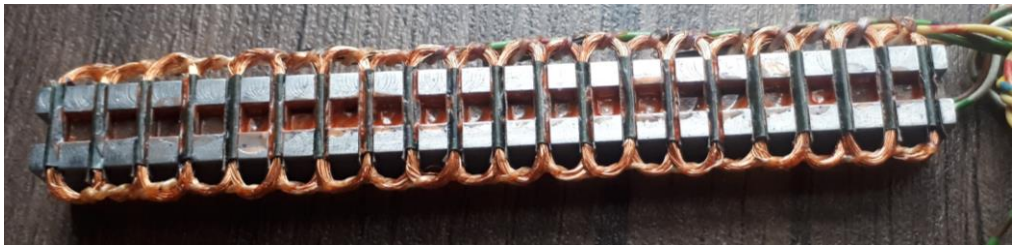

(a)

(b)

Fig. 9. Manufactured Resolver, (a): Primary, (b): Secondary

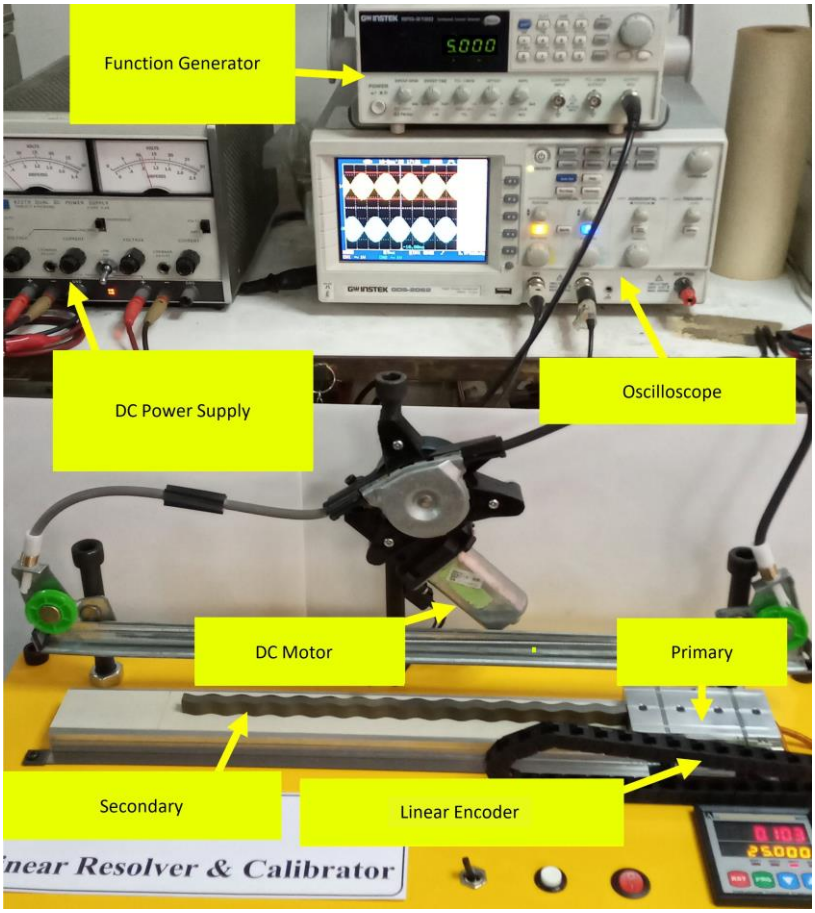

Fig. 10. Test system

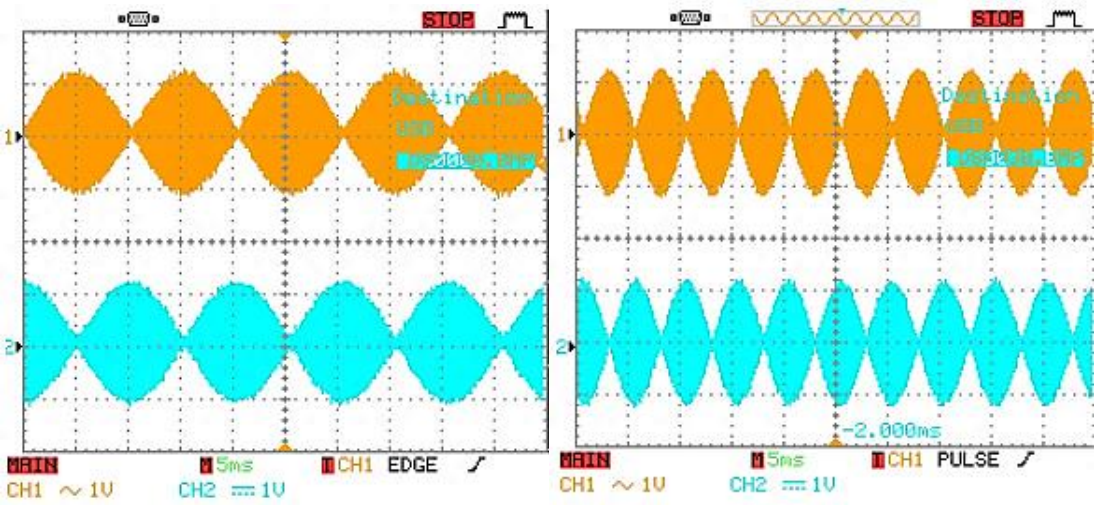

(a) (b)

Fig. 11. Induced voltages in AC excitation; practical results (a): 1 m/s, and (b): 2 m/s

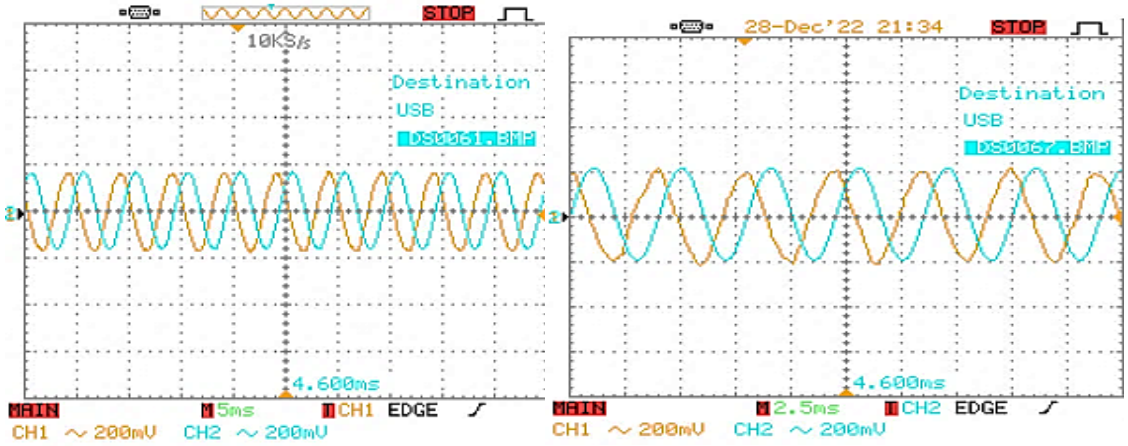

(a) (b)

Fig. 12. Induced voltages in DC excitation; practical results (a): 4 m/s, and (b): 5 m/s

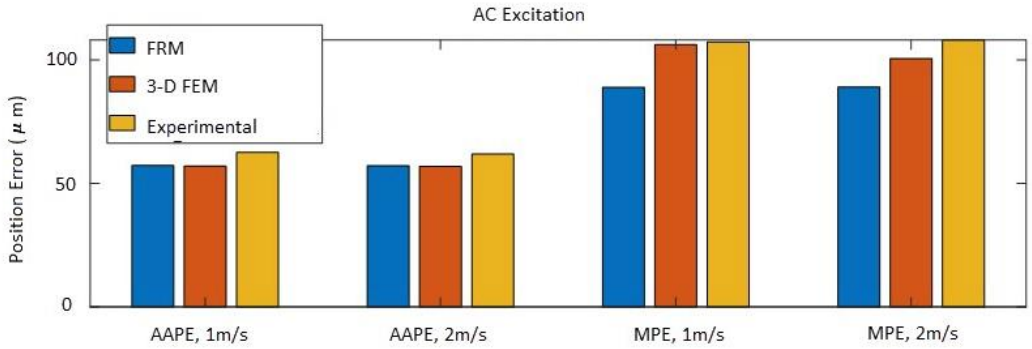

(a)

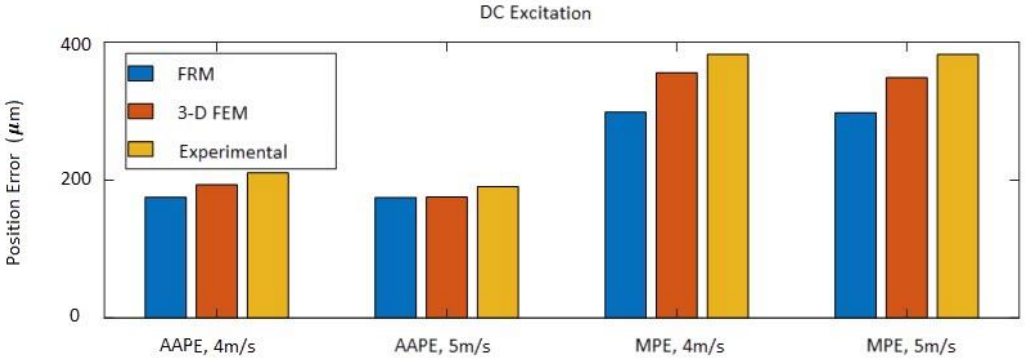

(b)

Fig. 13. Comparison of estimated position error resulted from FRM, FEM, and practical tests; (a): the results for AC excitation, and (b) the results for DC excitation

BIOGRAPHIES

Ghasem Salimi Moghaddam

Ghasem Salimi Moghaddam (Member, IEEE) received his B.Sc. degree in electrical engineering from Shahrood University of Technology, Shahrud, Iran in 2010, and his M.Sc. degree in electrical engineering with a focus on power electronics and electric machines from Sharif University of Technology, Tehran, Iran in 2023. His current research interests include the design, optimization, and performance analysis of electrical machines and electromagnetic sensors.

Zahra Nasiri-Gheidari

Zahra Nasiri-Gheidari (Senior member, IEEE) received the B.Sc. degree from the Iran University of Science and Technology, Tehran, Iran in 2004 and the M.Sc. and Ph.D. degrees from University of Tehran, Tehran in 2006 and 2012, respectively, all in Electrical Engineering. She is currently a Professor at the Department of Electrical Engineering, Sharif University of Technology. Her research interests include design, optimization, and performance analysis of electrical machines and electromagnetic sensors.

Ramin Alipour-Sarabi

Ramin Alipour-Sarabi was born in Iran, in 1989. He received the B.Sc. degree in power engineering from the Iran University of Science and Technology, Tehran, Iran, in 2012, the M.S. and Ph.D. degrees in power engineering both from Sharif University of Technology, Tehran, Iran, in 2014 and 2020, respectively. From 2021 he is an Assistant Professor with the Department of Electrical Engineering, K. N. Toosi University of Technology, Tehran, Iran. His research interests include the design, optimization, and performance analysis of electrical machines, machine drives, and electromagnetic sensors.